HST Spectroscopic Survey of the Symbiotic Stars

CHARLES D. (TONY) KEYES

Space Telescope Science Institute, 3700 San Martin Drive, Baltimore, MD 21218, USA; keyes@stsci.edu

We announce an HST survey of 18 symbiotic stars with STIS and present initial results. Eleven S-type symbiotics, six D-type symbiotics, and 1 D'-type symbiotic were observed in the survey. All but two stars were successfully detected. Ten of the objects observed had no previous usable ultraviolet observation. When combined with our contemporaneous ground-based optical spectra, our survey has increased the set of symbiotics for which quantitative models are possible by more than 50 percent. We report detection of resolved optical and ultraviolet subarcsecond-scale structures in the two nearest D-type symbiotics in the sample, V1016 Cyg and RX Pup. For V1016 Cyg our [O III] 5007 target acquisition imagery reveals subarcsecond-scale knots and structure in a roughly elliptical nebula approximately 1.″6 by 1.″0 in size. The central 0.″5 contains knots whose size and orientation are consistent with radio detections of structure. NUV Mg II spectral cross-profiles indicate subarcsecond bar-like structure in RX Pup similar to larger-scale optical and radio jet-like morphology previously detected from the ground. The bar in RX Pup is oriented with respect to the major axis of the radio and outer optical nebulosity in much the same manner as seen in HM Sge. No obvious extended features are seen in target acquisition imagery or spectra of any of the other stars in the survey, but detailed LSF/PSF fitting and spectral analysis remain to be performed and will be the subject of future work. Mg II imaging may be a promising tool for discovery of additional jets in symbiotic binaries.

Keywords: stars: binaries: symbiotics — stars: imaging — stars: individual (V1016 Cyg, RX Pup)

1 Introduction

The most complete compilations list approximately 150 known symbiotic stars (Kenyon 1986, Belczynski 2000). Approximately 30 additional symbiotic-candidate or symbiotic-related objects are also known. Of this set of about 180 objects approximately 75 were observed with IUE. Only 41 of those objects have spectra with any evidence of detection of an ultraviolet signal whether it be from continuum or emission lines. Only eighteen objects – about 10 percent of the entire sample – have sufficiently well-exposed SWP IUE continuum spectra to allow quantitative modeling of the hot components (Muerset et al. 1991). For that small subset of objects an amazing range of hot component properties has been determined:

$0.3\ L_\odot < L_{hot} < 37,000\ L_\odot$;
$55{,}000° < T_{hot} < 210{,}000°$;
$0.002\ R_\odot < R_{hot} < 0.8\ R_\odot$.

Together with my collaborators S. Kenyon (CfA), D. Proga (GSFC), R. Downes and W. Hack (STScI), and M. Gomez (U. Cordoba), we embarked on a combined HST snapshot ultraviolet and ground-based optical observational program designed to provide high quality (S/N $\sim$ 10-50 per pixel) observations at R $\sim$ 1000 from 1150 to 7000 Å for as many symbiotics as could be sampled by our HST snapshot program. The potential HST target list included 100 objects, which represented the entire set of objects accessible to STIS in one HST snapshot orbital visibility period.

Zanstra analysis of our observations will allow determination of hot component temperatures, luminosities, and radii. Optical and ultraviolet nebular diagnostics will yield T_e and N_e. Interstellar reddening will be determined from He II 4686/1640 ratios and the 2200 Å feature. Theoretical modeling will yield limits on red giant wind velocity laws and mass-loss rates. A substantial increase in the number of modeled symbiotics will lead to more meaningful statistical limits on the nature of hot component sources of ioniziation and fundamental wind parameters. Non-LTE models will assess the quality of traditional nebular diagnostics as applied to symbiotic systems and we expect to evaluate the correlation of observed electron densities with cool component types.

Symbiotic nebulae are formed by several processes such as fast winds from the hot components, slow winds from the cool components, photoionization processes, and in some cases shocks in colliding winds and outflows. Studying the extended nebular structure provides knowledge of the history of the mass-loss as well as its dynamics and geometry.

We provide a summary of our snapshot target list, observational limits, and survey observations. Additionally, we present initial quantitative results from our survey observations – the first visible and ultraviolet region detections of subarcsecond-scale structure for two important Mira symbiotics – V1016 Cyg and RX Pup. These observations have been serendipitously obtained as part of the spectroscopic survey of symbiotics with STIS.

2 Observations

Eighteen symbiotic stars were observed in our cycle 8 snapshot spectroscopic survey (program 8188) with STIS (see Table 1). Each observation began with a CCD visual region target acquisition image. A FUV/MAMA G140L ($\lambda\lambda$1150-1700 Å; 0.6 Å/pixel) science exposure was followed, in most cases, by a NUV/MAMA G230L ($\lambda\lambda$1700-3100 Å; 1.6 Å/pixel) science exposure. Spatial-dimension plate-scale is $0\farcs025$ per pixel in the MAMA exposures where a resolution element corresponds to two pixels in each dimension. Most of the spectra, including those discussed in this presentation, were obtained with the 52×0.5 slit ($0\farcs5$ slit width, $52''$ slit height). Detailed spectroscopic analysis of these observations will be presented elsewhere.

All eighteen objects were successfully acquired by STIS target acquisition procedures, however two of the objects (symbiotic-related objects RJ105 and UU Ser) were not detected spectroscopically (limiting $F_\lambda = 1 \text{ x } 10^{-16}$ erg cm^{-2}sec^{-1}Å^{-1}). Of the sixteen successfully detected objects, four have been modeled previously on the basis of IUE observations. The remaining 12 detected objects have never been modeled previously and ten of this set had never before been detected in the ultraviolet. As a direct result of our survey, we anticipate that the set of symbiotics with high quality hot component modeling will increase from 18 to approximately 30 objects.

Normally, STIS target acquisition observations are not intended to be deep exposures. They are designed as short-duration exposures that produce S/N$\sim$40 in the CCD image of the point source target. Spatial scale is $0\farcs05$ per pixel and a resolution element corresponds to two pixels. Most of our exposures used the broadband long-pass (λ > 5500 Å) F28X50LP filter which is not well-suited for detection of faint nebular emission in contrast to the strong red continuum light of typical symbiotic cool components. However, due to source brightness constraints three of our acquisition images were obtained with the F28X50OIII narrow-band interference filter (FWHM=6 Å; λ_c=5006 Å) which samples the light of [O III] 5007 Å at high contrast to the relatively faint cool component continuum. This filter has a modest infrared continuum leak.

3 Discussion

We measured the PSF of representative STIS point-source target acquisition images in the HST archive for targets with a wide range of color from O subdwarfs to late-type stars. We found no significant difference in the composite mean FWHM of the measured PSF for targets observed with either target acquisition filter. We found no color dependence in the results (F28X50III: 22 images FWHM = 1.71 +/- 0.18 CCD pixels; F28X50LP: 13 images FWHM = 1.68 +/- 0.14 CCD pixels). All of the 15 broadband symbiotic acquisition images and one of the three [O III] images (that for S149) had PSF FWHM within one standard deviation of the point-source means. The [O III] image of one object, V1016 Cyg, shows obvious resolved structure - see Figure 1 and discussion below. The FWHM of the [O III] image for RX Pup was 2 σ from the mean, however that particular image was so substantially underexposed that it does not present convincing evidence for extended nebulosity.

At the $0\farcs05$ per resolution element spatial scale of our two-dimensional MAMA spectra and our $52'' \times 0\farcs5$ slit size, we have ample capability for detection of extended subarcsecond structure in our spectra, as well. Careful PSF and LSF fitting remain to be performed for most of the spectra in our sample. However, the RX Pup NUV spectrum shows clear evidence of spatially-resolved subarcsecond-scale bar or jet-like structure (see discussion below).

3.1 V1016 Cygni

A cut of the intensity distribution of the F28X50OIII image of V1016 Cyg is shown in Figure 1. Substantial structure can be seen extending over a region approximately $1\farcs6$ x $1\farcs0$ with the long axis oriented approximately on the N-S line (P.A.$\sim$0°). The stellar point source, not visible in the cut in Figure 1, is found within the brightest feature, which is slightly asymmetric. In Figure 1 only the lower third of the brightness range is not saturated to accentuate the outlying structure. Inner region contours – also not shown in Figure 1 – seem oriented along the axis joining the

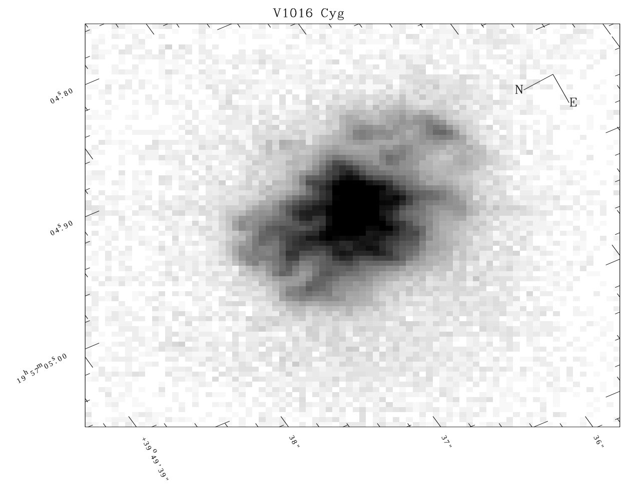

Fig. 1: STIS [O III] 5007 target acquisition image for V1016 Cyg. Logarithmic scaling of the brightness distribution is used on range 0-1000 counts (maximum level is 5900 counts) in order to allow outlying faint structure and filaments to be seen more clearly.

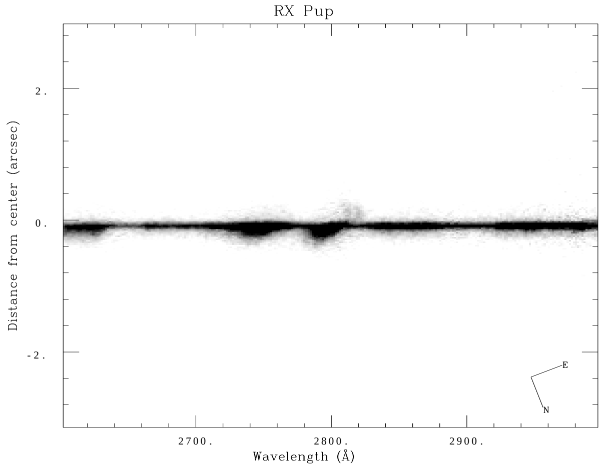

Fig. 2: RX Pup NUV G230L 2-dimensional spectrum image extract in wavelength range $\lambda\lambda$2600-3000 Å showing extent of asymmetric emission at Mg II 2800 and possibly Fe II 2750. Projected width of 52×0.5 slit is approximately 32 Å. Note the asymmetric spectrum cross-profile.

star and a knot (P.A.$\sim$40°). Amorphous emission extends in several directions from the center and several weak, outlying knots are visible.

The STIS [O III] filter has a red-leak longward of 10,500 Å for which the peak infrared transmission per Å, as given in the STIS Instrument Handbook (Sahu 2000), is $\sim$1% of the in-band transmission. Reference to IR observations of V1016 Cyg from the literature (Rudy et al. 1990), suggests that red-leak contamination in nebular line emissions due to He I 10,830 and Paschen γ is approximately 2% of the in-band [O III] 5007 strength. Similarly, signal due to out-of-band continuum light from the Mira component is approximately three times as strong as the weak in-band continuum signal. Red-leak contamination does not appear to be a significant contribution to the extended nebulosity detection.

Previous ground-based optical images obtained in [N II] 6584 and [O II] 3727 (Corradi et al. 1999) showed the existence of a 20$''$ diameter elongated nebula with major axis oriented at about P.A.=45°. Their images do show a knot and loop of emission approximately 3$''$ from an unresolved elliptical core, but importantly, none of their imagery resolves any structure within the central 3$''$ of the nebula. They also obtained an [O III] 5007 image, which showed no resolved nebulosity at all.

Several authors (e.g., Watson et al. 2000) have described subarcsecond radio structure. Much of the radio structure is resolved just at or below our 0.$''$1 resolution limit. Our interior knot and the central star asymmetry align with the Watson et al knots.

3.2 RX Puppis

The $\lambda\lambda$2700-2850 region of the two-dimensional NUV/MAMA spectrum of RX Pup is shown in Figure 2 with wavelength increasing to the right. The +Y axis of the 52$''$ $\times$ 0.$''$5 slit (up in the figure) is oriented on the P.A.=158° axis. The λ2796, λ2803 Mg II resonance doublet in emission, which is separated by slightly more than two spectral resolution elements, clearly shows evidence of a spatial elongation or bar from the "lower-left" to "upper-right" in the figure. The spatial extent perpendicular to dispersion of the short-wavelength component of the feature does not extend above the center line of the stellar spectrum. Similarly, the much weaker long-wavelength component of the feature does not extend spatially below the center line of the stellar spectrum. The feature appears to extend spatially approximately 0.$''$4 both perpendicular and parallel to dispersion along P.A.$\sim$115°.

Figure 3 shows an example of a strong Mg II emission feature in the spectrum of He2-38, another D-type symbiotic observed in our program which is an apparent point source – note the symmetry of PSF extension above and below spectrum center. Away from the bar-like features, the FWHM of the RX Pup stellar spectrum perpendicular to dispersion is approximately 4 pixels (0.$''$1), which is comparable to typical point-source cross-profiles such as that of He2-38.

The RX Pup Mg II feature does not completely fill the aperture along dispersion as the width of the entire feature is less than the 20-pixel width of the aper-

Table 1: HST Observations

Object	IR type	Acquisition Image	Spectra	Comment
V1016 Cyg	D	[O III]	FUV/NUV	subarcsecond-scale structure
RX Pup	D	[O III]	FUV/NUV	Mg II jet-like structure in NUV
S149	S	[O III]	FUV/NUV	no apparent structure
V741 Per	D'	broadband	FUV/NUV	no apparent structure
He2-38	D	broadband	FUV/NUV	no apparent structure
Hen 1591	S	broadband	FUV/NUV	no apparent structure
He2-156	S	broadband	FUV/NUV	no apparent structure
M1-21	S	broadband	FUV/NUV	no apparent structure
BX Mon	S	broadband	FUV/NUV	no apparent structure
SS29	S	broadband	FUV/NUV	no apparent structure
SS38	D	broadband	FUV/NUV	no apparent structure
BD−21°3873	S	broadband	FUV/NUV	no apparent structure
LMC-1	D	broadband	FUV/NUV	no apparent structure
Draco C-1	S	broadband	FUV	no apparent structure
V835 Cen	D	broadband	FUV	no apparent structure
UKS-Ce1	S	broadband	FUV	no apparent structure
UU Ser	S	broadband	no UV signal	good image; no apparent structure
RJ105	S?	broadband	no UV signal	good image; no apparent structure

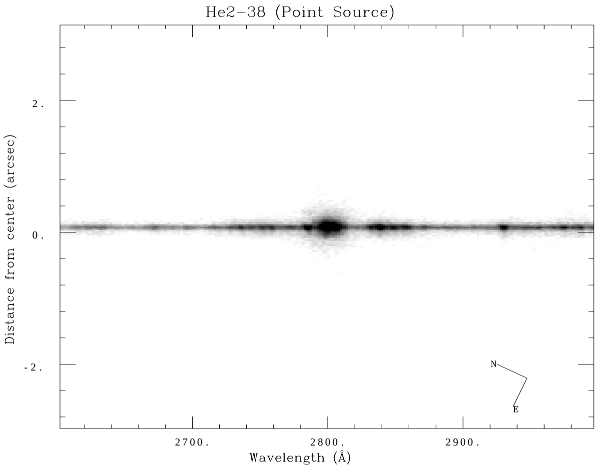

Fig. 3: Same type of spectrum image extract as for Figure 2, except for target He2-38. This object is another D-type symbiotic in our program. The spectrum cross-profile and emission line profiles are typical of point-sources observed with NUV G230L. The spectrum shows the extent and appearance of symmetric emission at Mg II 2800 – there is no evidence of extended structure.

ture. The feature may be produced by an extended jet-like structure oriented at approximately 45° to the +Y axis in the 2-dimensional spectrum, or along the P.A.=115° axis, with the stronger ("lower") component oriented to the WNW. The λ2756 Fe II feature also shows a similar, but weaker, structure, however C III] λ1909 and FUV emission features do not.

The Mg II feature is approximately $0\farcs55$ in length. For an estimated distance of 1 kpc, the projected physical length of this feature is ∼5500 a.u. Mikolajewska et al. (1999) estimate the binary separation at 17-50 a.u.

From ground-based [N II] 6584 and Hα coronagraph observations, Paresce (1990) reported the presence of a jet in RX Pup that extended from at least $1\farcs5$ to $3\farcs7$ projected distance from the central star along the P.A.=15° axis. A much fainter counter feature may also have been detected to the SW in the same images. This jet is co-aligned with the semi-major axis of an extended 60 mm radio emission nebula (Hollis et al. 1989) in the inner $1''$ circumstellar region. The orientation of the bar-like feature in our Mg II observations in the inner $0\farcs5$ is nearly perpendicular to the Paresce jet.

The Mg II bar in RX Pup lies perpendicular to the major axis of the radio and outer optical nebulosity in much the same manner as seen in HM Sge (Paresce et al. 1994). The asymmetric nature of the bar intensity distribution may be due to its large inclination to our line-of-sight with the SE side partially obscured by the inner regions of the system.

4 Summary

Initial examination of HST target acquisition imagery and ultraviolet spectra from our survey of the symbiotic stars has revealed the first visible and ultraviolet detections of subarcsecond structure in the well-known symbiotic Miras V1016 Cyg and RX Pup. We expect that the emission is from nebular material surrounding the system in the case of V1016 Cyg and is from an elongated bar or jet in RX Pup. This new structure appears to provide further evidence for the existence of elongated, collimated outflows in these two systems and should be an excellent tracer of such large-scale outflows.

Extended ionized nebulae seem to be a common feature of D-type symbiotic binaries. Based upon previous FOC observations of HM Sge and R Aqr (Paresce et al. 1994), our results here from RX Pup, and knowledge that the Mg II lines are often strong in S-type symbiotics as well, we suggest that ultraviolet Mg II imaging with HST would be an effective tool for discovery and study of additional jets in symbiotic binaries.

References

Belczynski K., Mikolajewska J., Munari U., Ivison R.J., and Friedjung M., 2000, A&A, 146, 407

Corradi, R.L.M., Brandi, E., Ferrer, O.E., Schwarz, H.E. 1999, A&A, 343, 841

Hollis, J.M., Yesef-Zadeh, F., Cornwell, T.J., Oliversen, R.J., Michalitsianos, A.G., Kafatos, M. 1989, ApJ, 337, 514

Kenyon S., 1986, *The Symbiotic Stars*, Cambridge University Press

Mikolajewska, J., Brandi, E., Hack, W., Whitelock, P.A., Barba, R., Garciz, L., Marang, F. 1999, A&A, 305, 190

Muerset U., Nussbaumer H., Schmid H.M., and Vogel M., 1991, A&A, 248, 458

Paresce F., Hack W.J., 1994, A&A, 287, 154

Paresce F, ApJ, 357, 231

Rudy, R.J., Cohen, R.D., Rossano, G.S., Puetter, R.C. 1990, ApJ, 362, 346

Sahu, K. 2000, STIS Instrument Handbook version 3, STScI, Baltimore, p. 365

Watson, S.K., Eyres, S.P.S., Davis, R.J., Bode, M.F., Richards, A.M.S., Kenny, H.T. 2000, MNRAS, 311, 449